RUSSELL L. McCALLY, RICHARD A. FARRELL, C. BRENT BARGERON,
HENRY A. KUES, and BERNARD F. HOCHHEIMER

NONIONIZING RADIATION DAMAGE IN THE EYE

This article describes a multidisciplinary research program to elucidate damage mechanisms in corneas exposed to infrared and microwave radiation and in retinas exposed to visible light. The approach combines physical science techniques, such as theoretical modeling and fluorescence spectroscopy, with biological techniques such as histology and specular microscopy. A new thermal model is used to explain the infrared damage, unexpected alterations in the cornea are found with low-level microwave exposures, and retinal damage is found to alter various fluorescence properties of diagnostic dyes.

INTRODUCTION

In many ways the eye is a unique organ in the body. The cornea and lens are optically clear tissues without blood vessels that normally remain with us throughout our whole life span, whereas other nonvascularized tissues, such as fingernails, hair, and even teeth, are often shed. The retina is formed early in the life of a fetus as an extension of the brain and retains many of the characteristics inherited in its origin. The retinal vascular system is the only such system in the body that can be seen clearly in vivo without any overlying opaque or translucent covering. Because of its unique characteristics, the eye is often examined as a means of diagnosing and studying the effects of many diseases such as high blood pressure, diabetes, sickle-cell anemia, and senility.

The anatomy of the eye, which is an almost spherical globe about 25 millimeters in diameter, is shown in Fig. 1 (top). The eye's optical system consists of the cornea, aqueous anterior chamber, iris, lens, and vitreous body, which are shown in cross section in Fig. 1 (center). The cornea, about 12 millimeters in diameter, supplies most of the refractive and light-gathering power. The lens is a variable power element that makes possible, at least in younger people, both near and distant vision. The iris varies the pupil size and hence regulates the amount of light entering the eye. The aqueous humor, almost entirely water, and the vitreous body, a gel-like substance, fill the spaces between the cornea and lens and the lens and retina. The retina is a many-layered photosensitive surface composed of nerve cells, photoreceptors, retinal pigment layers, and two separate vascular systems: the outermost choroid and the innermost retinal blood vessels. The sclera is the tough white protective layer covering the outside of the eye. In order for light to reach the retina in a useful manner, the optics must be clear and have the proper curvature. In order for light to be transformed into usable signals for the brain, all parts of the retina must be in functional order.

Because of its small size, fragility, and complexity, many parts of the eye and their functions are not completely understood. That understanding will require inputs from both physical and biological scientists. When the cooperative biomedical program between APL and the Johns Hopkins School of Medicine was first initiated, ophthalmologists from the Wilmer Institute had high expectations of a long-lasting relationship. From the beginning, this collaboration has received strong support from the University's administration and encouragement from the Navy, APL's principal sponsor. R. E. Gibson, F. T. McClure, and J. T. Massey at APL and A. E. Maumanee and A. Patz at the Wilmer Institute were particularly instrumental in the formation of the program that has lasted for over 20 years.

APL's Milton S. Eisenhower Research Center, especially the staff of the Theoretical Problems Group, has participated in collaborative studies with colleagues at the Wilmer Institute since the inception of the cooperative program. Several studies are active and were incorporated into the Group's biomedical section when the Research Center was reorganized in January 1984.

Our research efforts have centered primarily on the cornea and the retina. This article deals with the effects of nonionizing radiation on these tissues and with methods that can be used to characterize the morphological changes or damage that results from exposures to this type of radiation. The first section reviews our research on structural alterations in the cornea that are caused by the absorption of infrared radiation from carbon dioxide lasers. We discuss a new thermal-damage model for describing threshold damage to the cornea's front cellular layer. This model associates damage with the occurrence of a phase transition and provides a physical explanation for the small variation in the temperature rise that is calculated at the damage threshold condition for different exposure durations. The healing and repair processes that follow exposures above the damage threshold are also discussed in the first section.

The second section discusses morphological changes in the cornea's posterior cellular layer that are induced by exposures to low-level microwave radiation. Histological evidence suggests that significant numbers of

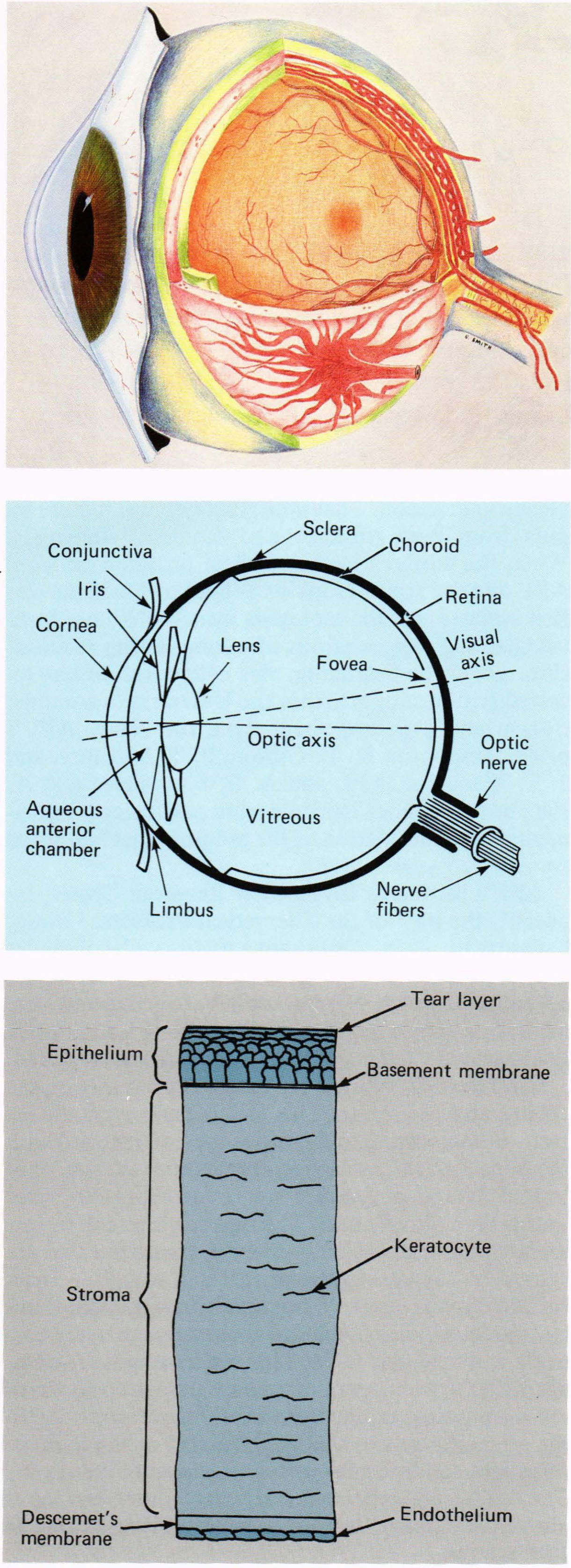

Figure 1—The eye. Top, anatomy of the eye; center, a diagram showing the important optical components; and bottom, a diagram showing the layers of the cornea.

these clinically observed lesions correspond to dead cells. These findings led APL to impose its own safe-exposure level for microwaves that is substantially lower than those currently recommended by the federal government. Finally, we discuss the inadequacy of present diagnostic methods for examining changes produced in the retina by low-level exposures to blue or violet light. The methods, which include retinal photography and fluorescein angiography, tell nothing of the mechanisms that cause these changes. We describe our development of new techniques, based on the measurement of several fluorescent properties of probe dyes, that show promise for uncovering the damage mechanisms.

STRUCTURAL ALTERATIONS IN THE CORNEA

The cornea is the transparent portion of the eye's tough outer coat (Fig. 1, bottom). In addition to passing light on to the photosensitive retina, the cornea, by means of its curved interface with the air, provides about 75 percent of the eye's focusing power. The cornea is a layered structure consisting of a connective tissue layer whose front and back surfaces are covered by cellular layers called the epithelium and endothelium, respectively. The epithelium is about six cells thick (≈ 50 micrometers), whereas the endothelium consists of a single layer of cells (≈ 5 micrometers). The integrity of these cell layers is essential for maintaining the health and transparency of the corneal stroma that they cover. The stroma accounts for 90 percent of the corneal thickness, which is about 500 micrometers in man and primates and about 400 micrometers in rabbits. The epithelial cells are firmly attached to the stroma by means of complexes in the very thin (0.05 micrometer) filamentous structure called the basement membrane. This membrane separates the epithelial cells from the stroma, and, at the back, a thin (≈ 10 micrometers) collagenous structure known as Descemet's membrane is located between the stroma and the endothelium.

The structure of the stroma, especially as it relates to corneal transparency, has been discussed in considerable detail in two previous articles in the *Johns Hopkins APL Technical Digest*.[1,2] For the purposes of this article, it is sufficient to note that the stroma consists of about 200 layers composed of parallel collagen fibrils. Between these layers lie a few cells called keratocytes, which occupy 3 to 5 percent of the stromal volume. Corneal transparency is the result of interference effects in the light scattered by the fibrils. These effects are due to short-range correlations in the positions of the fibrils about one another. The correlations are reduced if the cornea takes in water and then swells—a condition readily induced by damage to the limiting cellular layers and particularly to the endothelium. The resulting increase in light scattering causes a loss of corneal transparency.

Infrared Radiation Effects on the Cornea

Infrared radiation from a CO_2 laser operating at a wavelength of 10.6 micrometers is strongly absorbed by the water in the tear layer and in the cornea. Indeed, 99 percent of this radiation is absorbed in the first 48 micrometers of penetration, a region confined entirely within the epithelial and tear layers. Even with low-power lasers (< 1 watt), the absorbed energy can cause substantial temperature increases that lead to thermal damage of the epithelium, and heat conduction can spread the damage to deeper layers of the cornea, including the endothelium.[2-5] Thus, the ever-increasing use of CO_2 lasers by scientific research laboratories, by industry, and by the defense establishment and the concomitant increase in the chances for accidental exposure make it important to know damage threshold levels and to understand the mechanisms by which lesions are produced. Moreover, it is important to characterize the damage from exposures greater than threshold levels and to document the nature of the healing process that follows such wounds. This type of information lays the necessary foundations on which treatment methods can be based and their efficacy determined.

To gather this information, we initiated a multidisciplinary approach to examining corneal infrared damage. It consists of measurements of the exposure conditions that produce damage, theoretical calculations of the temperature-time histories caused by these exposure conditions, and documentation of the type of damage produced. The documentation consists of slit-lamp photography and histological examinations, including both light and electron microscopy of the damaged regions. The initial results of the program were reviewed in an earlier article[2] that covered damage thresholds for the corneal endothelium[3] and stromal cells[4] from single-pulse exposures, epithelial damage thresholds for both single- and multiple-pulse exposures, and measurements of temperature/time histories that were made to test the validity of our theoretical calculations.[5] In this article, we discuss additional research on epithelial damage thresholds from single-pulse exposures, outline the development of a new thermal model to explain the physical basis of this type of damage, and discuss the healing and repair processes that follow thermal wounds that extend about halfway through the depth of the cornea.

Threshold damage to the epithelium is characterized by a faint grayish-white spot on the surface of the cornea, visible in the slit-lamp microscope, that develops within one-half hour of the exposure.[6,7] Such a minor lesion will heal completely in 48 hours or less. Our previous research has suggested that such threshold damage, and indeed threshold damage of all corneal cells, is correlated with their experiencing a maximum temperature increase (calculated on the beam axis just below the corneal surface) of 40 to 45°C. The actual temperature increase depends weakly on the exposure duration and drops to about 36°C for exposures of 10 seconds or longer. We, and others,[7] call this empirical damage correlation a modified critical temperature model.

For damage threshold measurements, the CO_2 laser is operated in the mode that has a Gaussian irradiance profile (TEM_{00} mode) because that mode is reproducible and lends itself to analysis. Such an irradiance profile causes a radial temperature gradient on the cornea; thus, the peak beam irradiance (i.e., the value of the irradiance measured in watts per square centimeter on the beam axis) that is required to produce a given temperature rise on the beam axis at a given exposure time depends on the diameter of the beam.[3-5] Therefore, if the modified critical temperature model is valid, the peak irradiance required to produce threshold damage should depend on beam diameter in the same way. We have tested this hypothesis by determining the influence of beam diameter on damage threshold for three different exposure durations: 0.1, 1.0, and 10 seconds. The experimental results are shown by the data points in Fig. 2, where the measured peak irradiance

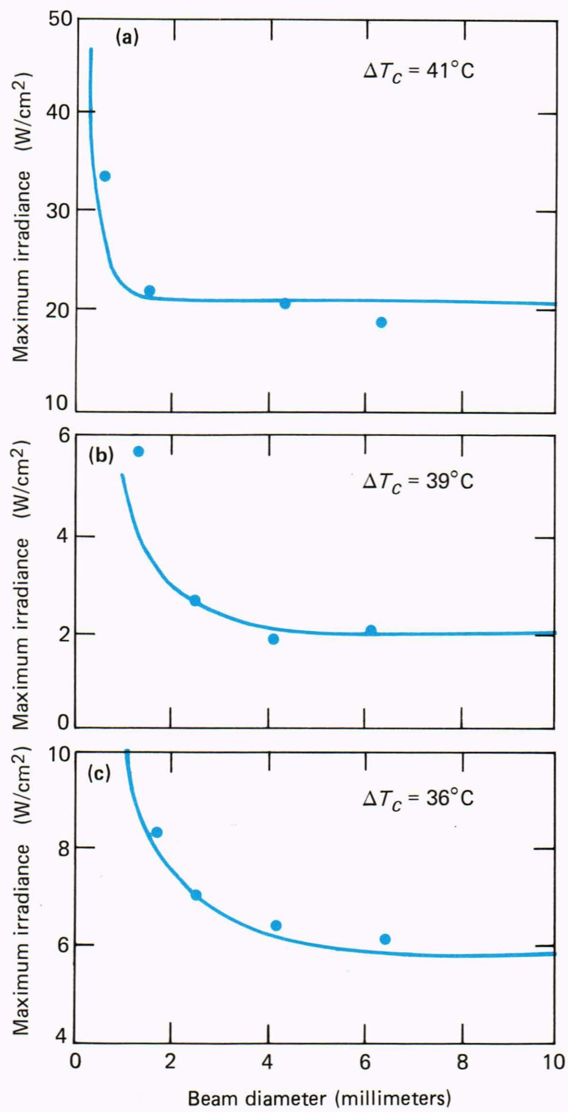

Figure 2—Data points are the peak irradiance required to produce threshold damage to the epithelium as a function of beam diameter. The exposure durations were 0.1 second in (a), 1.0 second in (b), and 10.0 seconds in (c). The curves are the calculated peak irradiances needed to produce a fixed temperature rise, ΔT_c, at a point on the beam axis 10 micrometers deep into the epithelium.

for threshold damage is plotted as a function of the beam diameter. Each of the three sets of data shows that the peak irradiance required for damage increases as the beam diameter decreases. This result is attributable to radial heat conduction in the cornea that becomes greater as the irradiated spot size decreases. If the modified critical temperature model is correct, then, for a given exposure duration, the measured peak irradiances should have produced a specific maximum temperature rise on the beam axis, independent of beam diameter. We checked the validity of this prediction by calculating, at each of the exposure durations, curves of the peak irradiance needed to produce a fixed temperature increase as a function of beam diameter. The experimental threshold damage irradiances could be fit by such curves, as is shown in Fig. 2. For the 0.1-second exposure, the solid line is for the peak irradiances that produce a 41°C temperature rise on the beam axis at a depth of 10 micrometers from the anterior tear surface. (The 10-micrometer value is chosen to be about 5 micrometers into the epithelium, considering that the average thickness of the tear film is about 5 micrometers. We have standardized our temperature calculations to that depth in order to have a consistent basis for comparison.) The solid lines through the 1.0- and 10.0-second data correspond to irradiances producing respective temperature rises of 39 and 36°C.

We also have continued to investigate the validity of the modified critical temperature model by extending the range of our measurements down to 1-millisecond pulses. The results of our single-pulse damage data are collected in Table 1. In Fig. 3 we have plotted the natural logarithm of the calculated peak temperature, ln T_c (on the beam axis, 10 micrometers below the corneal surface), that produces threshold damage as a function of the exposure duration. The initial surface temperature of the cornea was assumed to be 35°C. Although the values of ln T_c are nearly constant, as would be predicted by a critical temperature damage criterion, a slight downward trend can be discerned over the four decades in exposure duration. For the entire range, the temperature thresholds are fit by a modified (empirical) critical temperature in the mathematical form

$$T_c = 74\ t^{-0.018}\ °\mathrm{C}, \tag{1}$$

where the exposure duration, t, is in seconds. This relation is close to the one used by Egbert and Maher[7] to correlate corneal damage data from several laboratories.

To gain insight into the physical basis for the weak dependence of the critical temperature on exposure time, we have plotted in Fig. 4 the measured values of the energy density (measured in joules per square centimeter) required to produce threshold epithelial damage (ED_{th}) for these exposures as a function of exposure time. Since these values are experimental data, they are independent of any assumed thermal model. At short exposure times, the ED_{th} values appear to be asymptotic to a constant value, while for longer exposures, ED_{th} increases (nearly linearly on the log-log plot) with exposure time. This behavior might be expected if the occurrence of an endothermic phase transition within the epithelium were the underlying damage mechanism. In that case, a *thermally isolated* epithelium would sustain damage when it absorbed enough energy both to raise its temperature to the transition temperature and then to supply the latent heat needed to cause the phase change (e.g., protein denaturation or alteration of the organization of the lipids in the cell membranes). For such a thermally isolated epithelium, the

Table 1—Results of single-pulse damage.*

1/e Beam Diameter (mm)	*Peak Irradiance (W/cm²)*	*Exposure Duration (ms)*	*Energy Density of Damage Threshold (J/cm²)*	$\Delta T^{\dagger}_{max}$ *(°C)*
1.02**	624 ± 44	0.96	0.599 ± 0.042	54.0 ± 3.7
1.80**	175 ± 12	3.9	0.682 ± 0.048	46.5 ± 3.2
1.80**	62.9 ± 4.4	15.0	0.944 ± 0.067	41.3 ± 2.9
1.80**	50.9 ± 3.6	18.5	0.942 ± 0.066	38.0 ± 2.7
2.54**	57.2 ± 4.0	19.1	1.09 ± 0.08	43.6 ± 3.0
1.86	44.6 ± 3.1	31.0	1.38 ± 0.10	45.4 ± 3.2
1.56	21.9 ± 1.5	100	2.19 ± 0.15	42.0 ± 2.9
1.80**	9.01 ± 0.63	499	4.50 ± 0.32	38.2 ± 2.7
2.16	10.0 ± 0.7	500	5.00 ± 0.35	43.5 ± 3.0
2.44	6.52 ± 0.46	977	6.37 ± 0.44	38.7 ± 2.7
2.44	3.02 ± 0.21	9730	29.4 ± 2.0	36.0 ± 2.5

*For a Gaussian beam, the peak irradiance, I, is related to the total power, P, by $I = P/A_{1/e}$, where $A_{1/e}$ is the area of the beam at the $1/e$ radius. The energy density is the product of the peak irradiance and exposure duration. The error limits on the peak irradiance values are estimates that account for the final increments in the irradiance that were used to evaluate the actual threshold, and also for small fluctuations in laser intensity. These errors were used to set the error limits on the damage threshold energy density and the calculated value of ΔT_{max}.

**New data.

†Calculated at a depth of 10 micrometers from the anterior tear surface. This location is about 5 micrometers into the epithelium.

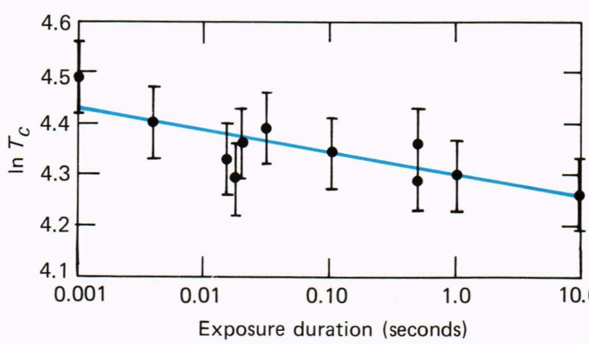

Figure 3—The calculated temperature 10 micrometers beneath the anterior corneal surface for single-pulse damage threshold exposures (cf. Table 1). The ambient temperature of the cornea surface was assumed to be 35°C. The line is a least squares fit to the data, yielding an empirical relation $T_c = 74\ t^{-0.018}$°C, where the exposure duration, t, is measured in seconds.

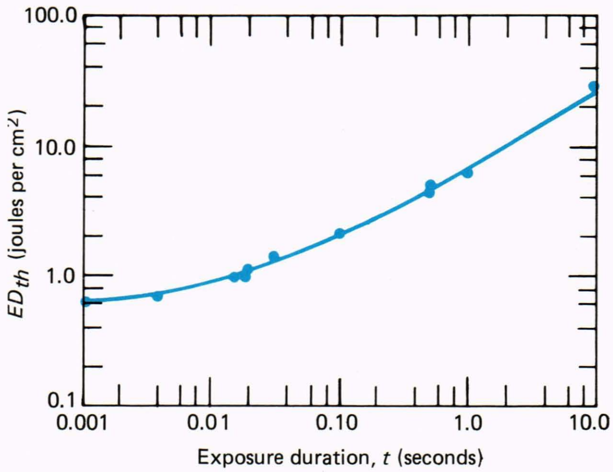

Figure 4—The energy density for threshold epithelial damage from single-pulse exposures as a function of exposure time. Note that the data appear to be asymptotic to a fixed value of ED_{th} for short exposure times. ED_{th} is a measured quantity and is therefore independent of any assumed thermal model.

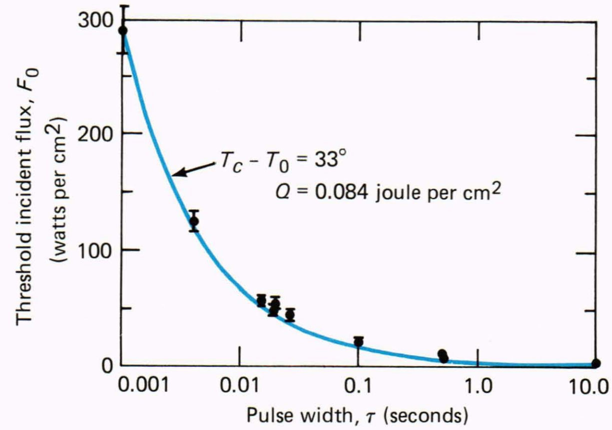

Figure 5—The data points are the experimental values of the effective flux, F_0, that produces threshold damage at the indicated single-pulse exposure durations. The error bars indicate the estimated accuracy of the flux measurement. The solid curve is the theoretical prediction from Eq. 2 for the indicated parameters. This figure suggests that all of the single-pulse data can be explained by a model that incorporates an endothermic phase transition.

ED_{th} value would be constant and independent of the exposure duration. In the actual epithelium, however, some of the energy would flow out because of conduction into the stroma. Thus, more energy would have to be supplied to compensate for that lost through conduction.

As a first step toward examining the possibility that such a phase transition is the underlying mechanism for the observed damage, we have considered a one-dimensional thermal model that corresponds to a uniform flux of heat, F_0, incident on a layered cornea whose initial temperature is T_0. We have further simplified the model by assuming that the incident flux is absorbed in an infinitesimally thin section at the anterior surface of the epithelium and by postulating that an endothermic phase transition occurs once the anterior surface reaches the transition temperature, denoted by T_c. The time at which this temperature is reached is denoted by t_c. We assume that the observed damage is associated with a specific amount of material per unit surface area undergoing the transition, i.e., after a specific quantity of heat per unit surface area, Q_c, goes into the phase transition.

For a pulse width τ (greater than t_c), the amount of heat per unit surface area that actually goes into the transition is obtained by integrating the difference between the incoming flux, F_0, and the quantity of heat per unit area conducted into the cornea, $-K\, \partial T/\partial x|_0$, from time $t = t_c$ to τ. Here, K is the thermal conductivity of the cornea, and the derivative is to be evaluated at the front surface. For this particular model, the integral can be done analytically, and the result is

$$Q = [(1 + \theta^2)\tan^{-1}\theta - \theta] \times \{[K(T_c - T_0)]^2\}/(2F_0\kappa) , \qquad (2)$$

where $\theta = [(\tau - t_c)/t_c]^{1/2}$, and κ is the thermal diffusivity. If the transition temperature, T_c, and Q_c were known, Eq. 2 could be used to predict the thermal flux of a uniform intensity beam that would produce threshold damage for a given pulse width τ. Although we do not know Q_c and T_c, we have elected to determine whether reasonable values for these parameters could lead to predicted values of thermal flux and pulse width that are in accord with the measured values of F_0 and τ at the damage threshold.

The actual data are for a laser beam having a Gaussian irradiance profile. As a first approximation, to incorporate the effect of the radial heat flow associated with the Gaussian profile into the present uniform beam problem, we chose an effective value of F_0 such that, in the absence of a phase transition, the calculated peak temperature at the end of the pulse would be the same as for the actual Gaussian beam. The data in Fig. 5 are the experimental values of the effective flux that produces threshold damage at the given pulse widths. The error bars are the estimated accuracy limits of the flux measurements. The curve gives the theoretical predictions of Eq. 2 for a transition that occurs at a temperature increase of 33°C and that has a value of $Q_c = 0.084$ joule per square centimeter. If a reasonable fraction of the epithelial material in the region of the wound, say 5 percent, undergoes the phase change, this value of Q_c would correspond to a latent heat of approximately 80 calories per gram, which is a physically reasonable value. These results suggest that endothermic phase transitions can explain the observed damge thresholds and account for the small variation of T_c with the exposure duration as noted in Fig. 3. In the future, we will extend these calculations to more realistic phase transition models that also account for the Gaussian irradiance profile and for multiple pulse exposures.

Corneas exposed above the threshold for epithelial damage but below that for endothelial damage develop a sharply defined bowl-shaped lesion, the borders of which correspond to a surface of equal peak temperature increase within the stroma.[2,4] The peak temperature value depends on exposure duration, being slightly lower for longer exposures. Since similar peak temperatures and dependencies have been found for threshold epithelial and endothelial damage,[2-5] we concluded that all corneal cells have the same thermal damage mechanism.

We have extended our work on this type of exposure in order to document the healing process. Lesions were produced in rabbits using a CO_2 laser operating in the TEM_{00} mode with the $1/e$ diameter of the beam set at 2.8 millimeters. The exposure was fixed at 25 watts per square centimeter (peak irradiance) for 0.4 second for the entire series of experiments. This exposure duration is about four times the threshold for epithelial damage (for this irradiance) and produces a wound that, at its deepest point, penetrates approximately halfway through the stromal thickness. Initially, 14 rabbits were exposed. Slit-lamp photographs were taken at 1, 24, and 48 hours and at 1, 2, 4, and 8 weeks after the exposures. The exposed corneas of two rabbits were prepared for histological examination at each of these intervals.

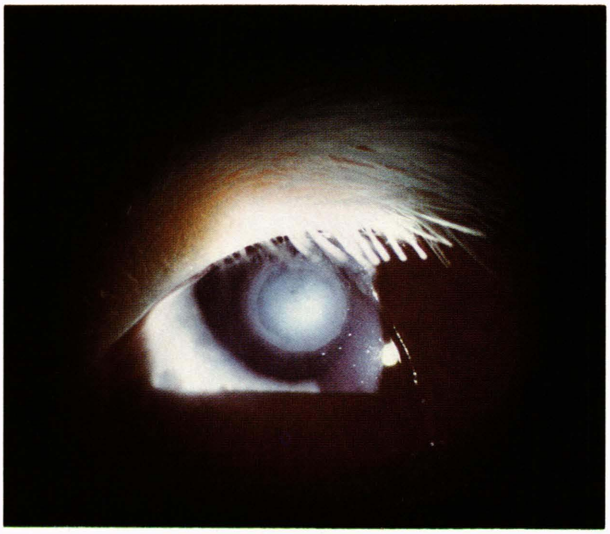

Figure 6—Slit-lamp photograph of a laser lesion 1 hour after an exposure that had a peak irradiance of 25 watts per square centimeter and a duration of 0.4 second. The $1/e$ diameter of the beam was 2.8 millimeters. This photograph shows the rough appearance of the coagulated epithelium in the center of the wound. The raised ring on the periphery of the lesion is typical for this exposure level.

Figure 6 shows the appearance of the cornea at 1 hour. The center of the wound is highly scattering, and the central cornea is thickened and rough. In addition, the coagulated epithelium is raised around the periphery of the lesion. There is a sharp transition from this damaged area to the clear, evidently undamaged, cornea. Light micrographs (not shown) confirm that (a) the damage extends about halfway through the stroma, (b) the endothelium and Descemet's membrane are normal, (c) the coagulated epithelium is about 60 percent of the thickness of the normal epithelium outside the lesion, and (d) the transition between damaged and undamaged epithelium is indeed very sharp. The electron microscope reveals that the epithelium shows marked disorganization, including nuclear chromatin clumping, loss of plasma membranes, and loss of cytoplasmic organelles (Fig. 7, top). Significantly, the basement membrane appears undamaged. The integrity of the basement membrane is essential for successful healing because damage to the basement membrane causes poor adhesion of the new epithelium as it grows to cover the wound. This can lead to delayed reepithelization, persistent defects, and recurrent epithelial erosion, or to even more serious complications such as stromal ulceration and perforation.[8] Higher magnification electron micrographs of the anterior stroma at 1 hour (not shown) reveal that the collagen fibrils have an abnormal fuzzy or smudged appearance.

By 24 hours, the coagulated epithelium has peeled off in about half of the exposed corneas, but even in those cases where it has not, the stromal lesion is already covered with a newly grown, but immature, epithelium that is only two cells thick. By 48 hours, the new epithelium is nearly as thick as normal, but the cells adjacent to the basement membrane still do not have their mature appearance.

We reported previously[2,5] that the bowl-shaped lesion in the stroma is devoid of cells 48 hours after exposure. The present experiments confirm that the stromal lesion remains acellular even 1 week after the exposure. However, by 1 week the corneal epithelium is completely normal and tightly adhering, which confirms that the basement membrane is not damaged at this exposure level.

By 2 weeks, the stroma is repopulated by keratocytes (Fig. 7, bottom), and other micrographs confirm that the stromal collagen has regained its normal appearance. At this time, however, slit-lamp examination reveals that the stroma is slightly thinned in the lesion area. This thinning results in the flattening of the anterior surface, a condition that persists throughout the remainder of the 8-week examination period. Figure 8 shows the appearance of the lesion in the slit lamp at 4 weeks. The flattening is evident in the narrow-slit view (Fig. 8, left), as is increased scattering, which is still evident in the anterior stroma. However, the lesion is only faintly visible with wide-slit illumination (Fig. 8, right). By 8 weeks, the lesion is difficult to locate with wide-slit illumination, but some increased scattering is easily noticed in narrow-slit views.

Significantly, no involvement of vascular components, such as monocytes or polymorphonuclear leukocytes, that are characteristic of an inflammatory response was observed during these experiments, nor was there any vascularization of the wound area. Also, the endothelium and Descemet's membrane remained normal throughout the 8-week period. We are examining a group of rabbits for possible long-term effects that persist beyond 8 weeks. In the future, we plan to

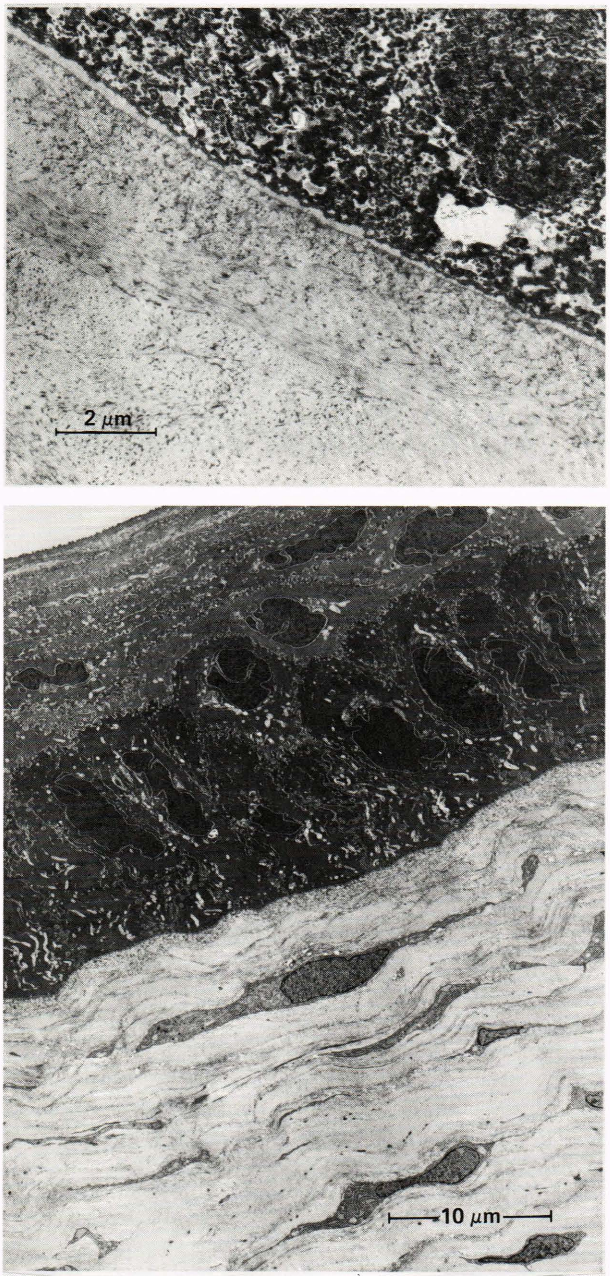

Figure 7—Electron micrographs of laser-induced lesions made at various intervals following exposures like that shown in the slit-lamp photograph in Fig. 6. The upper electron micrograph shows the epithelium and anterior stroma in the central lesion area at 1 hour. The epithelium shows marked disorganization, including nuclear chromatin clumping, loss of plasma membranes, and loss of cytoplasmic organelles. (For comparison, the bottom micrograph shows a normal epithelium.) The basement membrane appears to be undamaged. The lower electron micrograph shows the epithelium and anterior stroma in the central lesion area at 2 weeks. The stroma is repopulated with keratocytes.

investigate wound healing in the periphery of the cornea, which is in closer proximity to the vascular system, to discover if there is a lower threshold for an inflammatory response in that region.

Microwave Radiation Effects on the Cornea

Concern over the possibility of harmful ocular effects as a result of microwave exposure is not new. Indeed, there are several documented cases of opacities in human lenses that resulted from accidental exposure to microwave radiation.[9] Athough the threshold levels are not known for such cataract formation in humans, researchers have established a definite relationship between microwave exposure and cataract formation in test animals. The level of microwave exposure that produces cataracts in rabbits is about 0.10 watt per square centimeter, whereas the level required in primates is somewhat higher.[9] Most investigators believe that microwave cataracts are the result of a thermal damage mechanism.[9]

The original goal of our study was to determine whether observable retinal changes would occur in rabbit and monkey eyes after exposure to low-level (0.01 to 0.03 watt per square centimeter) microwaves. During the initial series of retinal testing, a new ophthalmic research instrument called a specular microscope was made available by the project's consulting ophthalmologist. The in vivo observations made with this instrument soon turned our attention from the retina to the cornea and launched us into a new and exciting project.

The use of specular microscopy began with the early slit lamp, an ophthalmic instrument used to view the cornea under low-to-moderate magnification. In 1968, Maurice[10] described the first laboratory specular microscope with magnification sufficient to resolve the individual components of an excised living cornea. Laing[11] and others modified the specular microscope to allow in vivo observation of the corneal endothelium. Figure 9 is a diagrammatic illustration of a specular microscope similar to that used by Laing. The specular microscope is described as an epi-illuminating microscope that projects a slit beam of light onto the posterior corneal surface at a nearly normal angle of incidence. Because of corneal transparency, most of the light entering is lost into and through the aqueous humor of the eye. However, a very small amount is reflected back into the cornea from the aqueous/cornea interface. A portion of this reflected light and backscattered light is gathered by the objective lens for imaging onto the film plane and for viewing.

The use of specular microscopy as a research tool to observe and photograph the endothelial cell layer in vivo was limited at first by the small number of endothelial cells that could be seen in each field of view. This limitation occurred because of the optical techniques employed to eliminate the interfering reflections of light scattered from the anterior surface of the cornea (epithelium).

To increase the area of endothelium that may be viewed, researchers such as Maurice[10] and Koester et al.[12] developed techniques and instruments with wider fields of view. These new instruments, and the one used in our study (Keeler-Konan), can view a 1- to 2-square millimeter area per frame.

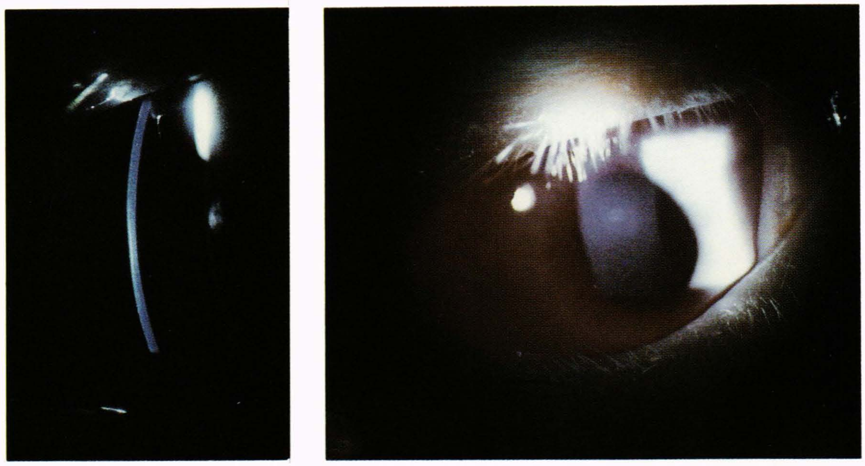

Figure 8—Slit-lamp photographs 4 weeks after an exposure like the one shown in Fig. 6. The narrow-slit photograph (left) shows the stromal thinning and the flattening of the anterior surface that first appears at 2 weeks, a condition persisting even at 8 weeks. The stromal scattering is reduced significantly from the levels at 1 and 2 weeks and is confined to the anteriormost region of the stroma. The wide-slit photograph (right) shows the slightly hazy appearance of the lesion. which, by 8 weeks, is barely noticeable.

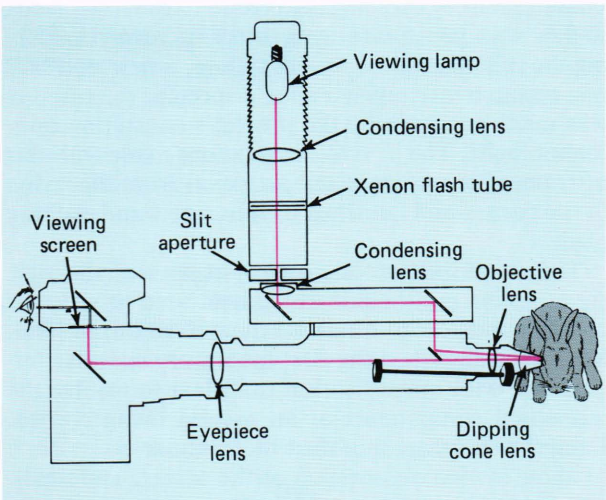

Figure 9—Diagram of a contact biospecular microscope similar to the type used to view monkey and rabbit corneal endothelia before and after microwave exposure.

In addition to the direct observation of endothelial lesions, specular microscopy is now used widely to assess such parameters as the number of cells per unit area or the frequency distribution of cell size in the corneal endothelium.[13]

Chemical or physical damage to the corneal endothelium is far more serious than to the epithelium, especially in humans and primates.[10] The epithelium in all species, when damaged, will normally repair itself in a rapid sequence of mitotic cell divisions as does the rabbit corneal endothelium. However, the endothelium of the adult monkey and human does not normally repair itself in this manner. Once endothelial cells of these species are damaged, they die and drop out, and the resulting lesions are filled in by surrounding cells that increase in size and migrate. This process results in an overall reduction in the cell population. Indeed, if enough endothelial cells are destroyed, marked swelling and loss of corneal transparency occur.

Thus, observation of lesions or altered structures in endothelial cells following exposures to microwaves at power densities very close to the recommended permissible exposure level takes on added significance. In the remainder of this section, we discuss the experiments that have produced lesions and the methods by which they can be observed and characterized.[14]

The apparatus we use for the animal exposures is shown in Fig. 10. The inside walls of the chamber are lined with microwave absorbing material. The chamber door is ventilated, and two air exhaust ports are located at the top of the chamber. The door ventilation and ports are carefully designed so that they do not introduce internal reflections of the microwaves. With this system, the internal chamber temperature remains within $\pm 1.5\,^{\circ}$C of the 23 to 25 °C room temperature during the 4-hour exposure sessions. Two types of microwave generators, both operating at 2.45 gigahertz, were used for the experiments. Continuous wave microwaves were generated by a Hewlett-Packard 8616B signal source driving an Alfred 5020 traveling wave tube (TWT) amplifier, while an Epsco PG5KB signal source was used to provide pulsed microwaves. The pulsed microwaves consisted of 10-microsecond-wide pulses at a pulse repetition frequency of 100 pulses per second.

The microwaves are transmitted through a coaxial cable to a bidirectional coupler to measure both forward and reflected input power. The microwaves from the bidirectional coupler then pass through a coaxial cable to a Hewlett-Packard S281A coaxial-to-waveguide transition source located within the anechoic chamber. For these experiments, the source with its 7.2- by 3.4-centimeter aperture was positioned over the ocular area to be irradiated with its long dimension centered above the nasal bridge at a height sufficient to allow a 10-centimeter gap between it and the ocular surface. This arrangement irradiated both eyes equally. The system input and reflected power levels were measured and recorded on a dual strip-chart recorder during each 4-hour exposure.

The microwave power density at the cornea was determined prior to each exposure with a Narda 8201

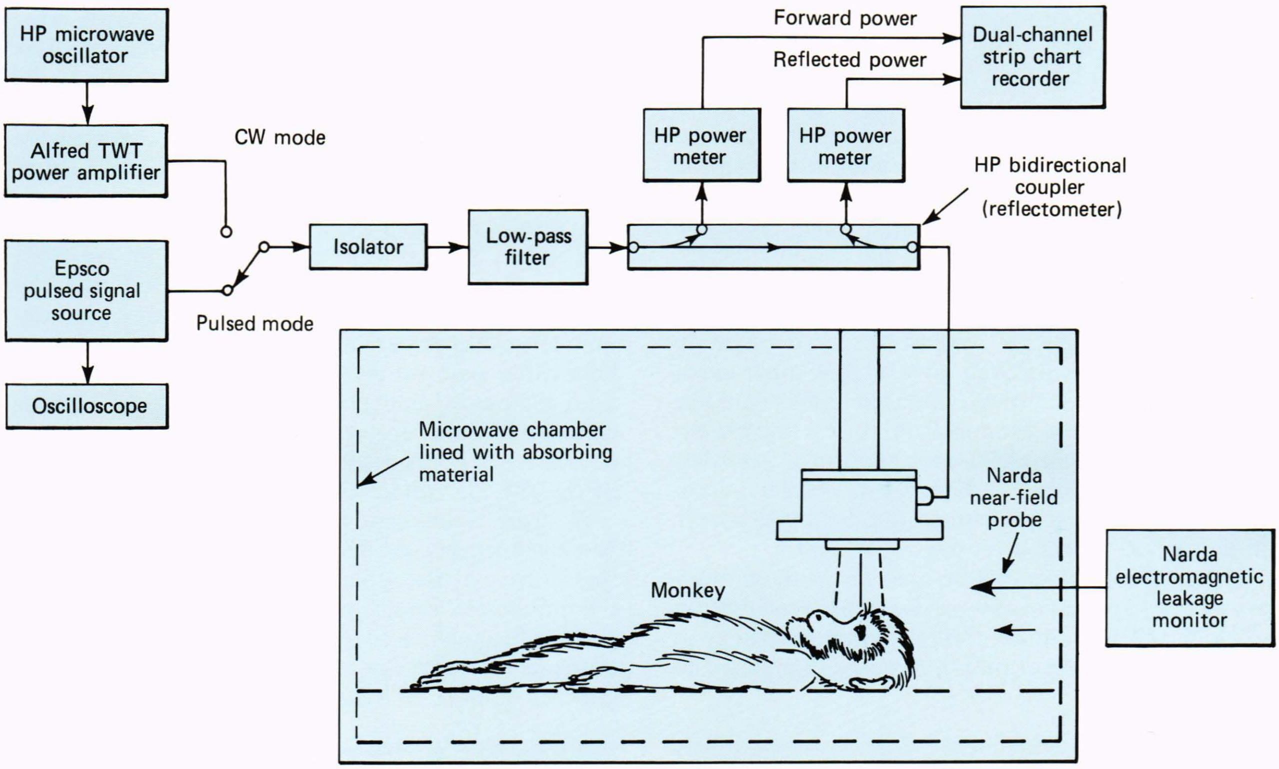

Figure 10—Microwave system used to expose the ocular area of anesthetized monkeys. The system can provide 2.45-gigahertz microwaves in either the continuous wave or pulsed mode.

electromagnetic monitor calibrated for 2.45 gigahertz. The probe was positioned at a point 10 centimeters from the source, approximating where the animal's nasal bridge and eyes would be located. These measured power densities were then compared with prescribed input power settings that had been obtained by means of an independent evaluation of the microwave delivery system. The evaluation included the measurement of transmitted power, antenna (emitter) gain and field pattern, various line losses, and component standing wave ratio.

Predicting the amount of energy absorbed by a specific part of the body during microwave exposure is a complex and often inaccurate procedure. Just knowing the amount of incident power to which a target organ is subjected is not sufficient to determine whether a temperature increase can be expected. To help quantify this dosimetric unknown, the National Council on Radiation Protection and Measurement proposed the specific absorption rate as a means of reporting microwave exposures in biological systems. Both "dose rate" and "density of absorbed power" are equivalent to the specific absorption rate. Each term refers to the amount of energy absorbed per unit time per unit volume, or per unit time per unit mass. The specific absorption rate may be simply defined as the time rate of energy transferred to the absorber by the electric field in the body. To convert our conventional incident power density readings (watts per square centimeter) into a more biologically significant means of reporting dosimetry (the specific absorption rate), in vivo temperature measurements were made during a 4-hour microwave exposure to 0.02 watt per square centimeter. A non-perturbing Fluoroptic (1000 B system) thermal probe was surgically implanted in the anterior chamber of the eye and butted up against the endothelial layer of the cornea. A baseline temperature of 34.5°C was recorded just prior to exposure. Microwaves with a power density of 0.02 watt per square centimeter were then applied as in a normal exposure session. The temperature was recorded every 4 seconds for the first hour and then every minute for the remaining 3 hours. A 1-minute temperature rise of 0.09°C was selected from the steepest part of the recorded 4-hour temperature increase of 0.77°C. This reading of 0.09°C per minute was then applied to the following equation, 1°C per minute equals 58.6 watts per kilogram, which is based on the tissue having a specific heat of 0.84 calorie per gram per degree centigrade. A calculated specific absorption rate of 0.26 watt per kilogram for each 0.001 watt per square centimeter of incident power was then assumed.

The experiments were performed on young cynomolgus monkeys. While in the microwave chamber, the monkeys were maintained under halothane gas anesthesia. They were in a supine position on a Styrofoam® platform, with both eyes (eyelids closed) directed toward the microwave source. As noted above, the animal was carefully positioned so that both eyes would be exposed equally.

Three exposure protocols were used. One involved a once-a-week, 0.005 to 0.03 watt per square centimeter exposure, lasting 4 hours and repeated over a period of time. Specular microscopic examinations were performed prior to any microwave exposure and then every 2 to 4 weeks thereafter until termination of the protocol. Another protocol involved a number of single 0.01 to 0.03 watt per square centimeter exposures of 4 hours separated by one or more weeks. Specular microscopic examinations were performed prior to each exposure and then at 4, 24, 48, and sometimes 72 hours after each exposure session. (Late in the study, after the discovery of a 16- to 48-hour latent period before the microwave-induced lesions could be observed, the 4-hour examination was discontinued.) In the final protocol, the 4-hour exposures were performed on 4 consecutive days, with specular microscopic examinations performed just before exposure on day 1 and repeated on days 3, 4, and 5.

These three protocols were used for both continuous wave and pulsed exposures. Controls were also run in which several monkeys were treated exactly as in the experiment, except that they were not exposed to microwaves.

The specular microscopic observations made prior to any microwave exposure always provided a clear view of normal hexagonally shaped endothelial cells having quite uniform sizes (Fig. 11, left). The cell boundaries were distinct and the nuclear regions were visible in most cells. The examinations performed at the various intervals following microwave exposure often revealed morphological changes in endothelial cells that were confined to areas that varied in size from one to several cells. Typically, there were multiple damage areas distributed over a damaged endothelium. The changes were never observed earlier than 16 hours after exposure and were sometimes not observed until 48 hours after exposure (Fig. 11, right). We concluded that the microwave effect has a latency period of at least 16 hours before it can be detected by means of the specular microscope.[14]

In order to evaluate the exposure conditions that produced lesions, we developed a grading scheme for the severity of the effect. The scheme was based on the number of lesions present in the standard photographic field (which covered 1 square millimeter of endothelial surface) for the eyes that contained the greatest number of lesions. Lesion severity was then

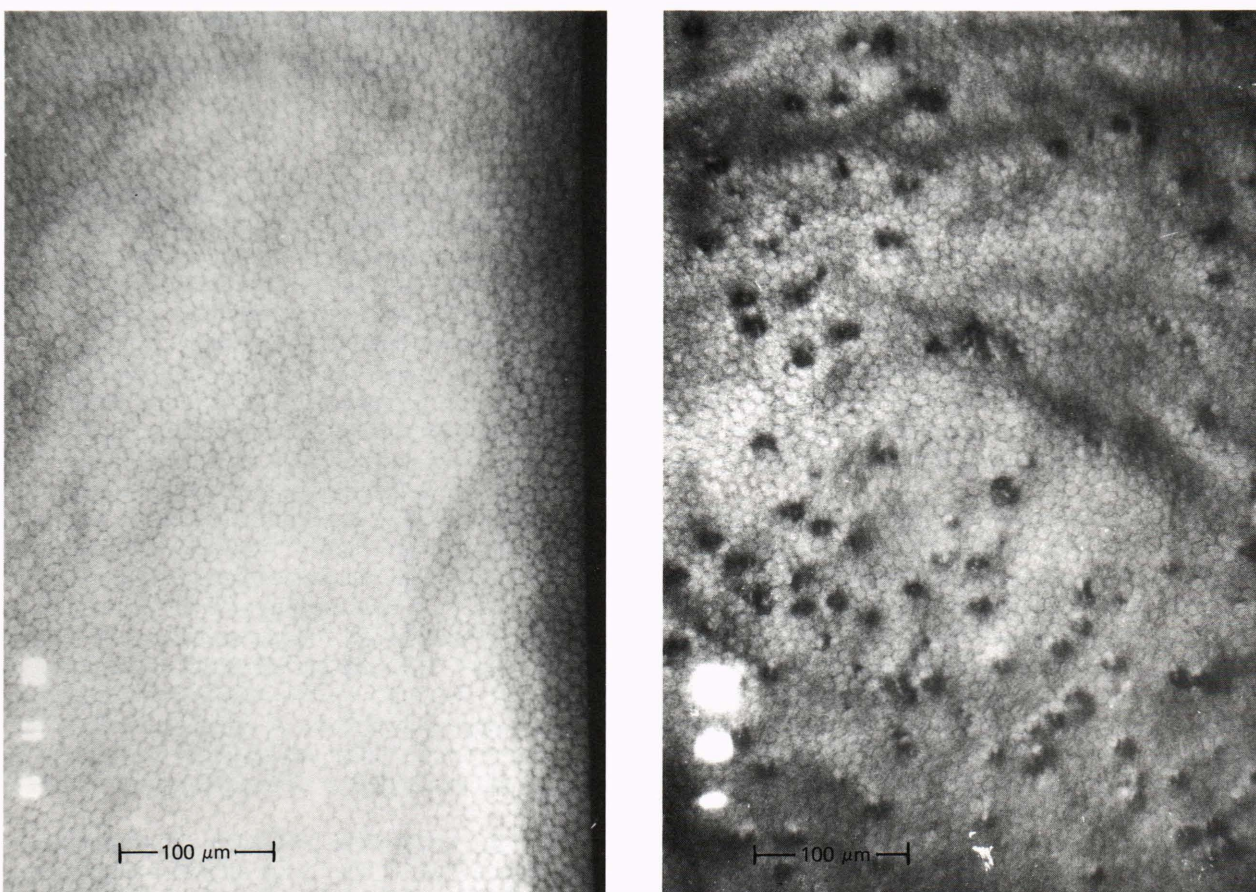

Figure 11—Left, a specular micrograph of the normal preirradiated monkey endothelium taken with a Keeler-Konan wide-field instrument. The cells are intact and healthy, with no lesions present. Right, a specular micrograph of a monkey corneal endothelium 48 hours after a 4-hour exposure to 2.45-gigahertz pulsed microwaves of 0.01-watt-per-square-centimeter average power. There are 50 or more lesions per square millimeter of corneal endothelium. The lesions vary from single-cell abnormalities to confluent abnormalities involving three or more cells. The lesions are scattered over the endothelium surface with intervening areas of normal-appearing corneal endothelium.

placed in one of four categories: no change, 0 to 2 lesions; minor change, 3 to 10 lesions; moderate change, 11 to 50 lesions; major change, more than 50 lesions.

The experiments show that the extent of the endothelial abnormalities is influenced by the power density, the type of microwave mode, and the exposure protocol (Tables 2 and 3).[14] Pulsed microwaves produced abnormalities at lower average power densities than corresponding continuous wave microwaves (Table 4). We found that a single 4-hour exposure to continuous wave irradiation (0.02 to 0.03 watt per square centimeter at 2.45 gigahertz) produced detectable morphological changes. Similar effects were observed following a single 4-hour exposure of 0.01 watt per square centimeter pulsed microwaves. While each exposure protocol produced at least minor changes under certain mode and power density conditions, major changes were most frequently observed with the protocol for which the 4-hour exposures were distributed over 4 consecutive days. No lesions were ever produced at the 0.005 watt per centimeter level with either microwave mode, nor were any lesions ever observed in the control experiments.

We have also performed histological examinations on several eyes after endothelial lesions had been observed in the specular microscope examination. For these examinations, we prepared one cornea for transmission electron microscopy, while the other cornea was prepared either for scanning electron microscopy or was examined using vital staining techniques. Transmission electron micrographs of the lesion area show prominent vacuoles within the endothelial cells and also show cells that have separated from Descemet's membrane. Descemet's membrane itself and the stroma appear normal. The scanning electron micrographs show areas of cell disruption ranging in size from one to five cell diameters (Fig. 12). The cells around these disrupted areas appear normal. We used a combination of two stains for the vital staining technique: alizarin red S outlines the cell borders, and trypan blue penetrates and thereby identifies dead cells. This vital staining confirmed the death or absence of endothelial cells in scattered areas such as those seen in the specular micrographs. Indeed, techniques that we have developed to correlate pathological findings with specular microscope observations[15] suggest that the lesions seen histologically correspond to some of the scattered lesions seen in the specular microscope.

In view of these histological findings, it is particularly interesting that specular microscopy done after the initial appearance of the lesions shows that they disappear after 72 to 96 hours. At that time, the endothelium appears essentially normal except for occasional large cells near areas where lesions had existed. Other areas where lesions had been present are populated by normal endothelial cells, which might suggest that in some cases the healing may have involved cell regeneration rather than the usual healing process in primates in which the cells enlarge and spread to cover the injured area. While specular microscopy is valuable in studying certain morphological features of the endothelium,[13] it is better to investigate the process of cell regeneration by autoradiographic methods. These methods measure the incorporation of tritium-labeled thymidine in endothelial cells.[16] Only newly formed cells (whose nuclei have newly made DNA) will contain the radioactive thymidine. We made autoradiographic measurements of flat-mounted corneal preparations. Epithelial sheets served as a positive control for the autoradiography, since epithelial cells are known to regenerate constantly to replace sloughed off cells. The epitheliuim, as expected, gave an excellent labeling index with a minimum of background grains.

Table 2—2.45-gigahertz continuous wave-microwave induced endothelium abnormalities (seven primates).

Exposure Levels (W/cm^2 avg.)	*Minimum Time Between Exposures*	*Number of Exposure Sessions*	*Number of Examination Sessions*	*Number of Times Abnormalities Observed*	*Degree of Change*
0.005	1 week	44	10	0	None
0.01	1 week	66	15	1	Minor
0.02	1 week	41	21	1	Minor
0.02	1 day	2*	2**	2	Major
0.03	1 week	14	12	5	Minor to major

*Each session consisted of four consecutive, daily, 4-hour irradiations.

**Effect first appeared between the third and fifth day after starting the protocol.

Table 3—2.45-gigahertz pulsed microwave induced endothelium abnormalities (eight primates).

Exposure Levels (W/cm^2 avg.)*	*Minimum Time Between Exposures*	*Number of Exposure Sessions*	*Number of Examination Sessions*	*Number of Times Abnormalities Observed*	*Degree of Change*
0.005	1 week	2	2	0	None
0.01	1 week	36	36	18	Minor to major
0.01	1 day	9	9	9	Major
0.010	Single exposure	2	2	2	Major

*Pulses were 10 microseconds wide and had a 100-pulse-per-second repetition rate.

Note: Equivalent specific abosrption rates are 0.26 watt per kilogram per 0.001 watt per square centimeter incident power density.

Table 4—Frequency of abnormalities.[14]

Mode	*Average Power Level (W/cm^2)*	*Total Observations*	*Times Damage was Observed*
Continuous wave	0.01 – 0.02	21	1
Continuous wave	0.02 – 0.03	27	7
Pulsed	0.01 – 0.015	38	20
Control	0	10	0

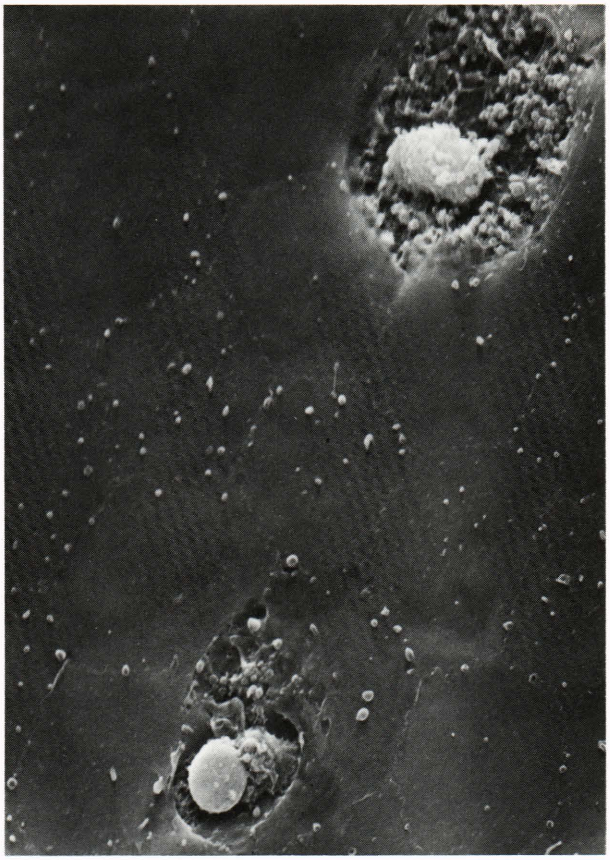

Figure 12—Scanning electron micrograph of a monkey corneal endothelium 48 hours after a 4-hour exposure to 2.45-gigahertz pulsed microwaves of average power of 10 milliwatts per square centimeter. Two cells are shown in the process of degeneration. Surrounding cells appear to be intact and healthy.

The six corneal endothelia that we examined showed no labeling. Thus we conclude that repair of the microwave damage occurs totally by spreading of surviving endothelial cells. These results suggest that not all of the morphological changes observed with specular microscopy correspond to dead cells; nevertheless, the histological results do confirm significant cell death. Since the lesions involving dead cells actually do heal entirely by cell enlargement and spreading, it is apparent that after repeated exposures the endothelial cell density would decrease.

Our experiments demonstrate that exposure to relatively low power microwave radiation can cause changes in, and even death of, corneal endothelial cells. The low power densities involved, together with preliminary measurements of temperature in the anterior chamber immediately adjacent to the endothelium, suggest that the mechanism is not thermal. At this stage of our research, however, we know little more of the actual damage mechanism. Several related factors also remain unclear. For example, the data for the protocol that involved repeated daily exposures suggest a possible cumulative effect. However, there is no evidence for a similar effect in the protocol involving single exposures spaced a week apart. We have also found, in separate experiments, that certain drugs (Pilocarpine and Timolol) that are applied in the form of drops appear to lower the threshold for the microwave-induced changes when they are instilled prior to irradiation. These drugs, which are used to treat glaucoma, are in widespread use; thus, this observation may prove to have significant clinical implications. Further investigations of the possible cumulative damage effect and the drug-related enhancement of damage may provide clues concerning the damage mechanism. Finally, it is important to document the effect on the cornea of chronic daily exposures over long periods of time. We have just begun to investigate such exposures and intend to discover whether endothelial cell density does continue to decrease to the extent that it results in corneal clouding.

The long-standing recommended permissible exposure level for microwaves in the United States was recently replaced. Previously, 0.01 watt per square centimeter was recommended as the maximum chronic exposure level for all microwave frequencies. This has been reduced to a recommended limit of 0.001 watt per square centimeter up to 1.50 gigahertz and to a limit of 0.005 watt per square centimeter beyond 1.50 gigahertz. Our data suggest an observable effect at approximately 0.01 watt per square centimeter for exposure to 2.45 gigahertz, which is quite close to the maximum level now recommended. On the basis of the histological findings in affected eyes, cellular changes might actually occur in the endothelium at exposure levels below the 0.01 watt per square centimeter level, even though they are not observable with the specular microscope. Thus, recognizing the fact that even the newly recommended maximum exposure levels may not provide a sufficient margin above those levels that produce a potential biological effect, APL has adopted its own safety standard for exposures to microwave radiation. The APL standard sets a chronic exposure limit of 0.0001 watt per square centimeter and applies to all employees, whether or not they work on microwave-generating devices.

EFFECT OF LIGHT ON THE RETINA

The retina of the eye is unique in that it is the only area in the body where blood vessels, both arteries and veins, can be clearly seen without any overlying obstructions. The retina can be examined through a dilated pupil by several types of ophthalmoscopes or by a slit-lamp microscope, and it can be photographed with a special camera called a fundus camera. (A fundus is the part of an enclosed cavity opposite an opening; the retina is the part of the eye opposite the pupil and hence the fundus of the eye.) Any of these instruments provide a slightly magnified view of the retinal surface. Figure 13 is a photograph of a rhesus monkey retina, which bears great similarity to a human retina. The optic disc, the macula, and the various arteries and veins of the retina are clearly displayed. In addition to these visual means of examining the retina, other measurements such as an electroretinogram (voltage

Figure 13—A retinal photograph of a normal rhesus monkey. The white area at the left is the optic disc or nerve head where blood vessels and the visual signals enter and leave the eye. Radiating from this area are the retinal arteries (the lighter-colored, smaller vessels) and the veins (the larger, darker-colored vessels). Near the center of the photograph is the macula, where high-resolution color vision takes place. A few (light pink color) choroidal blood vessels can be seen through the brown pigment epithelium that covers the retina everywhere except at the optic nerve.

Figure 14—A rhesus monkey retina with a phototoxic damaged area near the macula. Compare this with the same retina shown in Fig. 13.

response of the retina to light stimulation) can provide an indication of retinal function.

Damage to the Retina

We have had a long-standing interest in using optical methods to document retinal changes that are caused by exposure to visible or near visible light. One example of such a change is that caused by exposing the retina to high-intensity illumination of any wavelength of light where the optics of the eye are transparent. This type of change or damage is due to a 10°C or greater rise in temperature of the retina at the illuminated area. The mechanism is termed thermal, and such changes can be seen even during the irradiation period. Another type of change or damage is produced when the retina is irradiated for an extended time period with light that is blue or violet, at irradiation levels that are too low to produce any appreciable temperature rise. The exposure times are usually longer than 1000 seconds, and the retinal changes do not become visible in an ophthalmoscope until 24 to 48 hours after exposure. Figure 14 is a retinal photograph of the same monkey retina shown in Fig. 13, but after a 1-hour exposure that produced "blue light" damage. The lesion at the macular region was not visible until 2 days after the exposure and is still visible today, 3 years later. The mechanism causing these persistent "blue light" changes is unknown. Several investigators have postulated that either singlet oxygen or oxygen radicals are formed, and these substances subsequently destroy retinal tissue. It has also been proposed that the pigment epithelium, the scavenging system in the retina, becomes overloaded during the irradiation period to the point where tissue-destructive debris accumulates.

Fluorescence Photometry of the Retina

Fluorescein angiography provides another useful way to examine retinal integrity.[17] In this method, a solution of fluorescein dissolved in water is injected into a vein, and it circulates throughout the body's vascular system, including that of the eye. Sodium fluorescein, in solution, is highly fluorescent. As shown in Fig. 15, if such a solution is illuminated with blue light where it absorbs, it produces a bright green fluorescence. Thus, if the retina is illuminated by blue light, the fluorescence of the circulating dye can be photographed by a fundus camera equipped with suitable optical filters. Figure 16 is a fluorescein angiogram of the same monkey retina as in Figs. 13 and 14. The fluorescence of dye in the retinal blood vessels is easily seen. The underlying choroidal circulation is veiled but not completely obscured by the overlying pigment epithelium. Because sodium fluorescein is a small molecule (its molecular weight is 376) and because it does not bind tightly to proteins in the blood, it leaks from damaged or diseased blood vessels and therefore provides an ex-

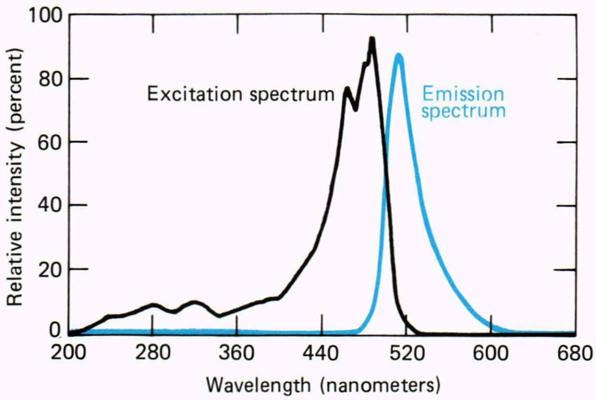

Figure 15—Fluorescence spectrum of fluorescein dye. The dye absorbs energy at wavelengths from 400 to 500 nanometers. Fluorescent energy is emitted from 500 to 600 nanometers.

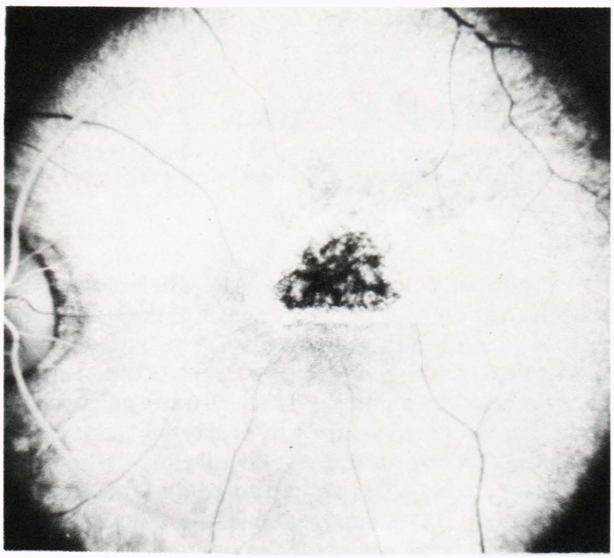

Figure 16—A fluorescein angiogram of the damaged retinal area of the monkey eye shown in Figs. 13 and 14. The damaged area has an increase in fluorescence over nondamaged areas.

cellent diagnostic tool. Note that in the Fig. 16 angiogram, it stains and outlines the light-damaged area of the retina. Sodium fluorescein is also nontoxic; it has been approved by the U.S. Food and Drug Administration for injection in human subjects and is used routinely in a clinical setting.

The in vivo tests that we have discussed so far enable only gross changes to be seen. At the present time, there is very little that can be ascertained at the cellular level of changes that occur in the retina with age, disease, or trauma except through histologic examination. Histology is obviously of no use in the prevention or early detection of retinal damage in humans. Our objective is to develop techniques to examine retinal damage at the cellular level in vivo. Such techniques should lead to a better understanding of the mechanisms producing damage and to improved prevention and treatment methods.

Cell biologists have devised powerful methods that use fluorescent dye probes to deduce information about the local environment of the probe.[18] Measurements of such quantities as excitation and fluorescence spectra, the quantum yield of the fluorescence, the fluorescence polarizability, and the fluorescence decay time are used in these methods.[19] In the remainder of this section, we will discuss how we have adapted a fundus camera to measure these quantities in the living retina. We will also discuss the methods we have been using to determine the usefulness of this type of data in analyzing retinal problems. Because it is already used for ocular tests, we have confined our studies to the use of fluorescein as the dye probe. Ultimately, we expect to be able to simplify the equipment and methods to the extent that they can be used in a clinical setting with human subjects.

The fluorescence of any molecule can supply information on processes that affect it during the time between excitation and emission of light. Although many types of fluorescent measurements can be made, the most difficult problem in the use of fluorescent probes is the recognition and analysis of the primary photochemical processes that are involved.[20] Figure 17 indicates what might happen when a dye molecule is excited by a photon. The dye molecule absorbs light, whereby a molecular electron is raised to an excited electronic level. This energy may reappear as heat in a radiationless decay, or it may be given up in normal fluorescence, or it may be transferred to a different electronic system. These various decay modes take place on widely different time scales.[21] Excitation takes place in 10^{-15} second (all times are approximate), and in 10^{-12} second the electrons undergo radiationless transitions to the lowest electronic level of the first excited state. If the dye is highly fluorescent, the electrons will most often return to the ground state in 10^{-8} second by emitting a photon of light.

Strongly fluorescent molecules almost always have singlet ground states and higher level triplet states. Some excited-state energy may be transferred to the triplet system in a reversible reaction. A triplet-state- to-singlet-ground-state transition is partially forbidden, which results in a long decay time (10^{-4} second). If the dye molecule is in close proximity to another molecule, the excited-state energy can be transferred to the nearby molecule. In solution, such transfers are generally controlled by diffusion, in which case a steady state is reached in 10^{-7} second. Some molecules (oxygen is of special importance in the eye) have triplet ground states and can, by energy transfer, deplete the dye molecule's triplet state. Since the excited singlet-state-to-triplet-state transfer of energy takes place in 10^{-8} second, a rapid depletion of the triplet state occurs, causing quenching of the primary fluorescence.

The basic fluorescent quantities of interest are the excitation and fluorescence spectra, the fluorescence quantum yield, the fluorescence polarizability, and the fluorescence decay time. Measurements of these quantities are used to infer the following conditions surrounding a fluorescent dye probe:

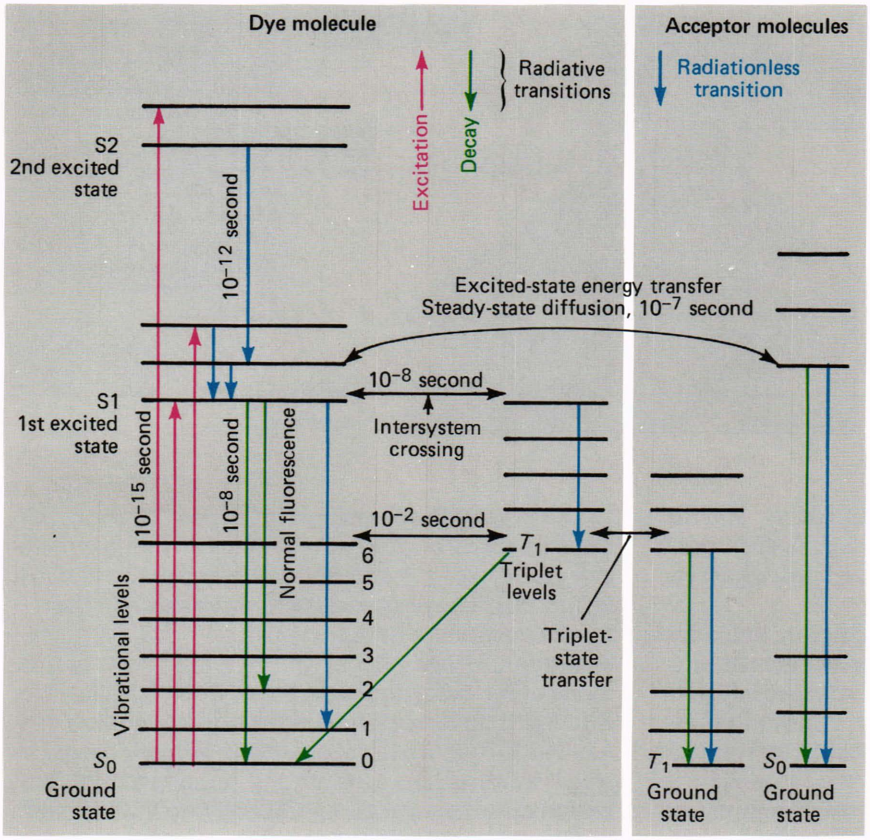

Figure 17—A fluorescent energy diagram shows some of the possible electronic levels for both a dye and an energy acceptor molecule.

1. *Binding Site Polarity.* The separation between the excitation and emission spectra is very sensitive to local solvent polarity. This information is of importance in understanding membrane transport phenomena.
2. *Environmental Constraints.* A viscous environment of the fluorescent molecule causes an increase in quantum yield and in polarizability. The polarizability can be used to infer the ratio of free-to-bound dye.
3. *Distance Measurements.* Electronic energy can be transferred between separated molecular systems. The rate of transfer is proportional to the inverse sixth power of the separation distance. The distances between binding sites of fluorescent probes can be inferred from measurements of the rate of transfer of fluorescence energy.
4. *Accessibility.* Fluorescence quenching can be caused by the presence of other reactive molecules. Oxygen is an important and powerful quencher. The exposure of the excited dye molecule to the quencher can be estimated by comparing the quantum yield of the free and bound fluorescent probes. Local oxygen partial pressure can, with suitable probes, be monitored with fast time resolution.
5. *Local pH.* Most fluorescent probes exhibited intensity and spectral changes with changes in pH. Thus, solution pH can be determined by measuring such changes.
6. *Heterogeneous Interaction.* Under favorable circumstances, several fluorescent decay times can be resolved. The existence of more than one characteristic decay time indicates multiple binding sites with different environments.

The optical system we have developed is a modified Zeiss fundus camera, shown schematically in Fig. 18. Light from either a monochromator or an argon ion laser illuminates a small area of the retina. The reflected or fluorescent light that is returned from the retina can go to either of two photomultipliers. One photomultiplier collects all of the light that returns from the retina; it is used to measure either the retinal reflectivity or the total fluorescent energy. The second photomultiplier has before it a rotating interference monochromator; it is used to measure either the fluorescence spectrum, the fluorescence polarizability, or the fluorescence decay time. Provisions are made in this modified camera for incorporating various polarizing elements or bandpass filters in either the input or output light paths. Stepping motors rotate the polarizing elements and the rotating interference monochromator. A computer collects data, controls the stepper motors, reduces the data, and displays the experimental results in either numerical or graphical form.

In a routine animal test, the retinal spectral reflectivity is measured and then fluorescein is injected into the test animal. At predetermined intervals after injection, the excitation and fluorescence spectra, the ret-

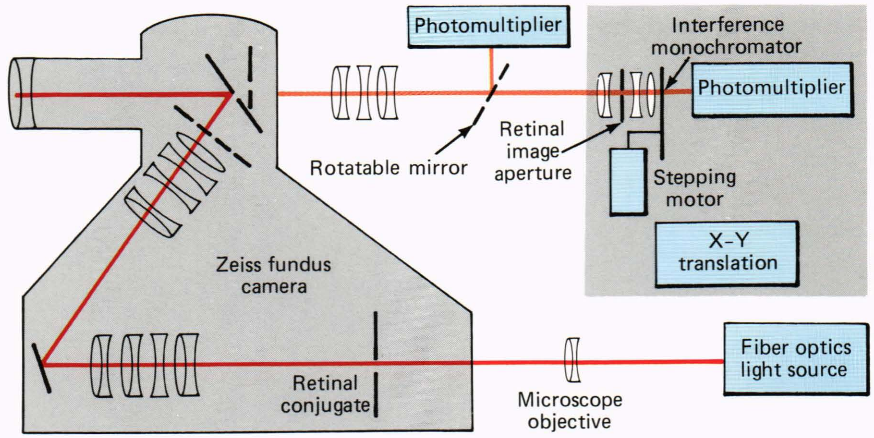

Figure 18—Diagram of the modified fundus camera that is used to illuminate the retina and to collect the return light for recording and analysis.

inal reflectivity, the fluorescence polarizability, and the decay time are measured, and the raw data are stored in the computer. After one to ten sets of measurements, the data are reduced.

The retinal reflectivity is measured before and after the fluorescein injection, and the decrease in reflectivity due to dye absorption is compared with the integrated fluorescence intensity to obtain the relative fluorescence efficiency. (Ideally, it would be better to measure the quantum efficiency of the dye; however, it cannot be determined because the absolute amount of light absorbed by fluorescein in the eye cannot be measured.) The excitation spectrum is obtained by comparing the total fluorescent output with the input power level to the eye from the monochromator. The fluorescence spectrum is measured with the rotating interference monochromator using the laser as the excitation source.

The fluorescence polarizability is defined as the ratio of the polarized component of the emitted light to the total emitted light when the excitation light is plane polarized. The fluorescence polarizability is derived from data obtained by polarizing the input energy and using a polarizer and a rotating quarter-wave plate in the fluorescent light path. In order to measure the fluorescence decay time, the argon ion laser beam is modulated at a high frequency by an acoustic optic modulator. The decay time is then derived from the phase delay between the modulated light from a fluorescent standard and the fluorescent light from the retina.

We have begun to test the system by measuring these various quantities in a normal monkey retina and in a light-damaged monkey retina. In addition, we measured the decay time in a normal monkey that was breathing oxygen and compared it to that in a monkey that was breathing an atmosphere rich in carbon dioxide. In order to have a baseline for comparison of data from these in vivo experiments, we have also made similar measurements on solutions of fluorescein in a wide variety of solvents. In solvents we can vary parameters (e.g., viscosity, pH, and solvent polarity) under controlled conditions. The results of the experiments are discussed in the remainder of this section.

The excitation spectrum is influenced by the conditions imposed on the ground state of the dye molecule. Of these, pH and polarity are usually the most influential. The peak excitation wavelength in the retina is consistent with a local pH of 7 and a dye concentration of one part in 10^6. We also find that the shape of the excitation spectrum of fluorescein in water is flatter than its spectrum in the normal monkey retina. The difference in shapes is not difficult to understand, however, since the absorption spectrum of most retinal absorbers varies significantly with wavelength in this spectral region.

The emission spectrum is influenced by conditions imposed on the excited state of the molecule, a state in which the equilibrium electronic configuration can be much different from that in the ground state. Thus, the local polarity, which determines the equilibrium configuration, often determines the peak emission wavelength. In the monkey retina, we found that the peak emission wavelength is 530 nanometers, the same value we found for a blood-fluorescein solution, and one that is considerably longer than the 520-nanometer value usually given for a water-fluorescein solution. This shift in the peak of the emission spectrum is consistent with a high local polarity. Since this degree of polarity is only found inside cells, these data provide strong evidence that the fluorescein has penetrated cell membranes. In addition, the shapes of the emission curves from both the water-fluorescein solution and the retina are similar and consistent with the lack of a significant population of the triplet state.

The fluorescence intensity is influenced by polarity, pH, and molecular binding sites. Since the pH in the retina is probably around 7, the maximum intensity is expected. It is not possible to measure the absolute amount of fluorescence in the retina of an intact eye; however, we do find that the fluorescence intensity from fluorescein in blood is less than half that of fluorescein in water, a result that is indicative of an especially large binding-site influence.

The quantum efficiency is determined not only by the intrinsic efficiency but also by any packing constraints or by changes in the geometry of the upper state during the period when the fluorescent molecule is excited. As noted above, we measure the ratio of the integrated intensity to the integrated increase in absorption. Although this is not the quantum efficiency, the two quantities are closely related. We find in the normal retina that the ratio decreases with time after fluorescein is injected into the circulation. We interpret the decrease as resulting from a change in the packing constraints with time. If the dye molecules come very close together, dye complexes called dimers can be formed that have low quantum yields. Indeed, this is the reason usually given for the decrease in fluorescence intensity when a dye is in a very concentrated state.

The separation between the peak of the excitation spectrum and that of the fluorescence spectrum is influenced by the viscosity of the medium, but even more by any intersystem triplet-state excitation that occurs when the molecule is in the excited state. In a water solution, this separation is 8 nanometers, whereas it is 38 nanometers for fluorescence from the normal monkey retina. The large increase indicates that there is a moderate-to-large amount of intersystem crossing and hence a relatively large number of molecules being transferred to the triplet state. The lack of any triplet-state emission spectrum (which we noted previously) indicates that the triplet state is quenched, probably by oxygen.

The fluorescence polarizability of dye molecules in solution is determined by the solution viscosity. For bound dye molecules, the size, shape, and flexibility of the binding molecule determine the polarizability. The fluorescence polarizability in a monkey retina is 9.6 percent for excitation and 8.8 percent for emission, for an average of about 9 percent. These are preliminary measurements and have not been corrected for such known effects as light scattering in the eye and the fact that the cornea and lens are birefringent. However, the values are probably not in error by more than 20 percent. With this in mind, we have estimated the ratio of bound to free dye. An equation relating the polarizability to the ratio of bound to free dye can be derived in the form

$$\frac{C_b}{C_f} = \left(\frac{I_f}{I_b}\right)\left(\frac{p-p_f}{p_b-p}\right) ,$$

where C_b/C_f is the ratio of bound to free dye, I_f/I_b is the intensity ratio for free to bound dye, p is the measured polarizability, p_f is the polarizability of free dye, and p_b is the polarizability of bound dye. Our measurements indicate that C_b/C_f is 0.64, i.e., about 70 percent of the dye is free and about 30 percent is bound. Others have stated that as much as 80 to 90 percent of fluorescein injected intravenously is bound to blood proteins. If this same value held true in the retina, we would have measured a polarizability close to 33 percent. We must conclude that the amount of unbound dye in the retina is much higher than the value previously determined for blood proteins.

If the fluorescence emission is not quenched by other nearby molecules, the decay time measures the natural fluorescence lifetime. If fluorescence quenchers are present, the decay time is shortened. In most biological systems, molecular oxygen is the most important fluorescence quenching agent.

We have measured the decay time of fluorescein fluorescence in water, in blood (oxygenated and deoxygenated), in a normal monkey retina, and in a light-damaged monkey retina. The decay time that we measured in water compares favorably with published data when instrumental effects are properly taken into account. We found that the decay time in blood is shorter than it is in water and, much to our surprise, that it is independent of the blood's oxygenation state. This lack of change in the decay time, when taken together with the lesser fluorescence intensity in blood than that in water, indicates that some of the fluorescein dye molecules do not contribute to the fluorescence. This could happen in several ways. For example, the nonfluorescent fluorescein molecules are either in a very acid local environment, or the hydrogen atoms have been stripped away (as in an alcoholic solution), or the dye structure is changed (as in the change from the fluorescein molecule to the almost identically structured nonfluorescing phenolphthalein molecule). The remaining fluorescein molecules that contribute must be shielded from oxygen. It is likely that this happens because the oxygen is bound to hemoglobin.

On the other hand, we have found that the fluorescence decay time of fluorescein in a normal monkey's retina is much shorter than in blood and is affected significantly by the animal's oxygen intake. These retinal measurements suggest a high degree of quenching and that the dye molecules are not bound. We note that our fluorescence polarization data from the retina also indicate a low degree of binding. The fact that blood has little effect on the intrinsic decay time of fluorescein (compared to its decay time in water), when taken together with the lack of dependence of decay time on blood oxygen content, must mean that the significant changes with oxygenation that are seen in the retina must be due to fluorescein that has found its way outside the bloodstream.

Fluorescence measurements taken on a burn-damaged area of the retina show that the intensity increases and the polarization and the decay time decrease. We have not yet obtained good excitation and emission spectra for such retinas. The intensity and polarization changes indicate an increase of unbound dye, and the decay time change indicates an increase in quenching. Any explanation of the changes that occur in a damaged as opposed to an undamaged area of the retina would be very speculative at this stage of our research.

Other than the normal problems that are encountered in any experimental development procedure, such as increasing the accuracy and decreasing the system complexity, there are problem areas specific to this type of experiment. The retina is a heterogeneous collection of molecules. We measure the fluorescence of fluorescein in the vicinity of many of these different molecules, and thus the measurement represents an average value. We also do not know exactly where the fluorescein that we see is actually located in the retina. Some is in the blood system, some is absorbed on membranes, and some penetrates inside various proteins. Our efforts to locate the site of fluorescein in the retina have been unsuccessful so far. Also, the eye tissues have wavelength variations in light absorption, reflection, and scattering that are not well known and that vary drastically from animal to animal and species to species. Such variations influence the fluorescence measurements. When we can solve these as yet intractable problems and determine rate equations for all of the energy pathways that occur in the fluorescence process in both normal and abnormal retinas, we will be able to determine in detail some of the changes that occur in the retina due to disease or trauma.

In addition to these "big" problems, there are innumerable other engineering problems. At present, only one small area of the retina is sampled. This is acceptable only if retinal damage can be easily seen; it would not be acceptable for preventive diagnostics. In order to measure all of the desirable fluorescence quantities, the elapsed time exceeds 6 minutes, which is too long when multiple measurements are needed after a single fluorescence injection. If these measurements are to be made on human subjects, it will be very desirable to reduce the light levels to an absolute minimum in order to obtain maximum patient cooperation. Finally, all of the fluorescence data will have to be corrected for artifacts introduced both by the instrumentation and by the eye itself.

We are optimistic that, in time, all of these problems will be solved and that fluorescence photometry will become a useful tool in the field of ophthalmology.

REFERENCES

[1]R. W. Hart, R. A. Farrell, and M. E. Langham, "Theory of Corneal Structure," *APL Tech. Dig.* **8**, 2-11 (1969).

[2]R. A. Farrell, C. B. Bargeron, W. R. Green, and R. L. McCally, "Collaborative Biomedical Research on Corneal Structure," *Johns Hopkins APL Tech. Dig.* **4**, 65-79 (1983).

[3]C. B. Bargeron, R. A. Farrell, W. R. Green, and R. L. McCally, "Corneal Damage from Exposures to Infrared Radiation: Rabbit Endothelial Damage Thresholds," *Health Phys.* **40**, 855-862 (1981).

[4]R. L. McCally, C. B. Bargeron, W. R. Green, and R. A. Farrell, "Stromal Damage in Rabbit Corneas Exposed to CO_2 Laser Radiation," *Exp. Eye Res.* **37**, 543-550 (1983).

[5]C. B. Bargeron, R. L. McCally, and R. A. Farrell, "Calculated and Measured Endothelial Temperature Histories of Excised Rabbit Corneas Exposed to Infrared Radiation," *Exp. Eye Res.* **32**, 241-250 (1981).

[6]A. S. Brownell and B. E. Stuck, "Ocular and Skin Hazards from CO_2 Laser Radiation," in *Proc. 9th Army Science Conf.* pp. 123-138, AD-785609 (1974).

[7]D. E. Egbert and E. F. Maher, *Corneal Damage Thresholds for Infrared Laser Exposure: Experimental Data, Model Predictions, and Safety Standards,* U.S.A.F. School of Aerospace Medicine, Brooks AFB, SAM-TR-77-29 (1977).

[8]J. A. Fogle, K. R. Kenyon, and W. J. Stark, "Damage to Epithelial Basement Membrane by Thermokeratoplasty," *Am. J. Ophthalmol.* **83**, 392-401 (1977).

[9]S. F. Cleary, "Microwave Cataractogenesis," *Proc. IEEE* **68**, 49-55 (1980).

[10]D. M. Maurice, "The Cornea and Sclera," in *The Eye*, Vol. 1B, H. Davson, ed., Academic Press, Orlando (1984).

[11]R. A. Laing and W. M. Sandstrom, "In-vivo Photomicrography of the Corneal Endothelium," *Arch. Ophthalmol.* **93**, 143-145 (1975).

[12]C. J. Koester, C. W. Roberts, A. Donn, and F. B. Hoefle, "Wide Field Specular Microscopy: Clinical and Research Applications," *Ophthalmology* **87**, 849-860 (1980).

[13]L. W. Hirst, C. Auer, H. Abbey, J. Cohn, and H. A. Kues, "Quantitative Analysis of Wide Field Endothelium Specular Micrographs," *Am. J. Ophthalmol.* **97**, 488-495 (1984).

[14]H. A. Kues, L. W. Hirst, S. A. D'Anna, and G. Dunkelberger, "Effects of 2.45 GHz Microwaves on the Primate Corneal Endothelium," *Bioelectromagnetics* **6**, 177-188 (1985).

[15]L. W. Hirst, W. R. Green, and H. A. Kues, "Clinical Specular Microscopic/Pathologic Correlation," *Cornea* **2**, 159-164 (1983).

[16]N. L. Mills and A. Donn, "Incorporation of Tritium Labeled Thymidine by Rabbit Corneal Endothelium," *Arch. Ophthalmol.* **64**, 443-446 (1960).

[17]A. Wessing and G. Von Noorden, *Fluorescein Angiography of the Retina,* C. V. Mosby Co., St. Louis (1969).

[18]A. A. Thaer and M. Sernetz, eds., *Fluorescence Techniques in Cell Biology*, Springer-Verlag, New York (1973).

[19]S. Udenfriend, *Fluorescence Assay in Biology and Medicine,* Academic Press, New York, Vol. 1 (1964); Vol. 2 (1969).

[20]N. J. Turro, *Modern Molecular Photochemistry*, The Benjamin/Cummings Publishing Co., Inc., Menlo Park (1978).

[21]C. A. Parker, *Photoluminescence of Solutions,* Elsevier Publishing Co., London (1968).

ACKNOWLEDGMENTS—The investigations of corneal infrared damage are supported by a contract from the U.S. Army Medical Research and Development Command and by Independent Research and Development (IR&D) funds. Special appreciation is owed to Owen J. Deters at APL for his work on the thermal damage models and to W. Richard Green at Johns Hopkins' Wilmer Institute for his expert analysis of the histology produced in his laboratory by Zenaide DelaCruz. Also at APL, Stanley Favin continues to help greatly in the computational phases of the work. Finally, we thank Edwin Beatrice and Bruce Stuck of the Army Institute of Research for continuing support and insightful discussions. The microwave research has been supported by the Office of Naval Research and by IR&D funds. It is a pleasure to acknowledge the contributions of Lawrence Hirst, presently at Washington University, to these studies. The fluorescein dye work was supported by IR&D funds and by Wilmer Institute departmental funds. That project is indebted to Arnal Patz for his encouraging support and to S. A. D'Anna for his aid with animal care and anesthesia.

THE AUTHORS

RUSSELL L. MCCALLY (second from right) was born in Marion, Ohio. He received the B.Sc. degree in physics from Ohio State University in 1964 and shortly thereafter joined APL's Aeronautics Division, where he was involved in research on explosives initiation. In 1969, he joined the Theoretical Problems Group in the Milton S. Eisenhower Research Center. He received the M.S. (1973) and M.A. (1983) degrees in physics from The Johns Hopkins University, and in 1979-80 was the William S. Parsons Fellow in the Physics Department. Mr. McCally's research interests include the application of light scattering methods to the study of corneal structure, corneal alterations from infrared radiation, and magnetism in amorphous materials. He is co-principal investigator on a National Eye Institute grant that supports corneal light scattering research. His professional memberships include the American Physical Society and the Association for Research in Vision and Ophthalmology.

RICHARD A. FARRELL's biography can be found on p. 72.

C. BRENT BARGERON (left) joined APL in 1971 as a member of the Research Center. Born in Provo, Utah, in 1943, he earned a Ph.D. degree in physics at the University of Illinois in 1971, where his thesis was on high-pressure physics. Since joining APL, Dr. Bargeron has been involved in problems in solid-state physics, light scattering, chemical lasers, arterial geometry, corneal damage from infrared radiation, mineral deposits in pathological tissue, spectrometry of several types, and surface science.

HENRY A. KUES (second from left) joined APL in 1965 as a member of the Milton S. Eisenhower Research Center and has been with the Theoretical Problems Group since 1984. Born in Baltimore in 1946, he studied chemistry and biology at Essex Community College and The Johns Hopkins University. He is a senior staff engineer and a research associate in ophthalmology at the Johns Hopkins School of Medicine. His research interests include the effect of microwaves and other forms of nonionizing radiation on biological systems.

BERNARD F. HOCHHEIMER (right), a member of the Principal Professional Staff and a physicist in the Theoretical Problems Group of the Milton S. Eisenhower Research Center, was born in Rochester, N.Y. He received the B.S. degree in physics (1951) at St. Bonaventure University and the M.S. degree in optics (1953) at the University of Rochester. He joined APL in 1954 as an associate physicist. From 1956-60, he was employed as a scientist by the Hayes Aircraft Corp., where he was involved with infrared physics. Since rejoining APL in 1960, he has been conducting research on fluorescein angiography, laser retinal light damage, spectroscopy, and related ophthalmological and biomedical problems. Mr. Hochheimer holds a patent on angiography of the separate retinal and choroidal circulations and is a member of the Optical Society of America.